Theoretical and Applied Fracture Mechanics 117 (2022) 103144

Contents lists available at ScienceDirect

Theoretical and Applied Fracture Mechanics

journal homepage: www.elsevier.com/locate/tafmec

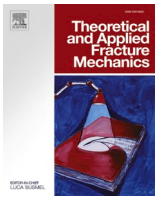

A fretting fatigue model based on self-steered cracks

Diego Erena [a,*], Jesús Vázquez [a], Carlos Navarro [a], Jaime Domínguez [a,b]

[a] Universidad de Sevilla, Escuela Técnica Superior de Ingenieros, Departamento de Ingeniería Mecánica y Fabricación, Camino de los Descubrimientos s/n, C.P. 41092, Spain

[b] Laboratory of Engineering for Energy and Environmental Sustainability, Universidad de Sevilla, 41092 Seville, Spain

ARTICLE INFO

Keywords:
Fretting fatigue
Fatigue life model
Fatigue crack initiation
Fatigue crack propagation, crack path

ABSTRACT

In this article a new fretting fatigue life prediction model is presented. The model can be classified as a variable crack initiation length: the crack initiation and crack propagation phases are calculated as a function of the crack initiation length, and among all the feasible crack initiation lengths and orientations, that producing the minimum fatigue life is considered. In this new proposal the crack direction is automatically determined as a function of fatigue parameters in both phases: initiation and propagation. The model is applied to a wide experimental campaign of fretting fatigue tests, and excellent correlation is obtained between experimental and predicted fretting fatigue lives and crack paths.

1. Introduction

Fretting fatigue is a common material damage in many engineering components. It appears in mechanical joints that are subjected to time variable forces/moments. Under such loading conditions, small oscillating relative displacements between the contacting surfaces arise. These relative displacements, in junction with friction between the contact pair, produce small surface cracks [1]. In many situations, these time-varying forces include a bulk stress in the component, that is responsible for a more accelerated crack propagation process. In such circumstances the phenomenon is termed fretting fatigue [2–4].

Fretting is a problem concerning many aircraft components, in especial it is of high importance at disk-blade joints in aero gas turbines [5,6]. Due to this fact, in the last two decades a considerable amount of fretting fatigue life assessment models have been proposed. The variety of fretting fatigue models is wide, but as a rule of thumb a major division can be done between those models considering only the crack initiation phase [7–11], those that only take into account the crack propagation phase [12–15] and models that combine both phases [16–21]. These models use normally any variant of the ε-N curve to assess the crack initiation fatigue life and linear elastic fracture mechanics (LEFM) to estimate the propagation life. One difficulty that arises in any fatigue model is the election for the crack initiation length, a_i, considering this length as that at which crack nucleation/initiation finishes and crack propagation starts. Most fatigue models, whether taking into account only one or both fatigue phases, consider a fixed crack initiation length, which is usually based on the El Haddad characteristic length, a_0 [22], defined as a property of the material. Besides, in some models that combines crack initiation and propagation phases, the length considered to average some fatigue parameter to evaluate the initiation cycles does not math with the crack length considered to assess the subsequent propagation phase [21]. This is due to the difficulty of establishing an objective definition to the phases appearing during the total life of a crack. The model proposed in the current paper, avoids the explicit definitions of nucleation, initiation and propagation. To do so the model directly combines the available fatigue and fracture techniques, such as ε-N curves and their variants and LEFM, to obtain the crack combination that minimizes the life of the component. Obtaining, as part of the process, a crack length that delimits two phases. A first phase corresponding to a nucleation and growth of microcracks which will be called as initiation phase and a second phase corresponding to a crack growth of greater length cracks which will be called propagation phase.

In addition, and more specifically related to the fretting case, the majority of proposed life assessment models assume that the crack is perpendicular to the contact surface, both in the crack initiation and/or propagation phase. This hypothesis has yielded good results in terms of life prediction [19]. Nevertheless, is not realistic on the basis of experimental observations that show how cracks emanate and propagate with a certain angle with respect to the surface [24].

In previous authors' works, have been developed models that combines crack initiation and propagation phases but "automatically" selects the crack initiation length a_i [17–20], although the crack is

* Corresponding author.
E-mail address: deg@us.es (D. Erena).

https://doi.org/10.1016/j.tafmec.2021.103144
Received 14 September 2021; Received in revised form 25 October 2021; Accepted 25 October 2021
Available online 29 October 2021

assumed to be perpendicular to the surface in both phases. Later, new approaches - based on multiaxial fatigue critical plane parameters- were proposed by authors in order to predict the initial fretting fatigue crack path [23,24], or the posterior crack propagation path [25], but in those works no attempt was done to predict the fatigue life. More recently, both the crack initiation and propagation phases were modelled considering that the crack can take an arbitrary angle with respect to the surface, but the crack initiation length was fixed to a certain value [26].

Due to the multiaxial and non-proportional stress/strain state in fretting, especially at the near-contact surface material, it is a common practice the use of multiaxial critical plane approaches in order to predict/simulate the crack initiation phase. Among the wide variety of available multiaxial critical plane parameters, the Fatemi-Socie (FS) [27] and Smith-Watson-Topper (SWT) parameters [28] are frequently used in fretting models. The manner in which the fatigue parameters are used in order to predict the crack initiation phase is quite diverse: in some works the value at a material point is calculated [10,16,18,29], in others a mean value over a line, area or volume is considered [9,19,30], approaches that, from a physical point of view, are more in agreement with the crack initiation fatigue process. On the other hand, crack propagation phase in fretting is usually modelled via fracture mechanics approaches [10,12–14,19,20,31,32]. Regarding the crack path, in the specific case of fretting fatigue, previous work has demonstrated a better correlation of the predicted crack paths when using the SWT parameter compared with the FS parameter [23,25]. Initial crack paths predicted by the SWT parameter are in very good agreement with those obtained experimentally. The SWT parameter is able to capture the slight slope of cracks with respect to the surface transversal direction (cracks pointing inside the contact zone). However, the FS parameter estimates cracks with erroneous orientations and pointing outside the contact zone.

In view of the previous authors' works, the present one can be considered as an extension of all them. As in previous works, in this one both crack initiation and crack propagation phases are combined in order to obtain a non-fixed crack initiation length a_i, but here the crack direction, in both fatigue phases, is automatically determined as a function of the SWT multiaxial fatigue parameter, and thus leading to a "self-steered crack" fretting fatigue model. The proposed model is applied to a wide experimental campaign of fretting fatigue tests, and very good results are obtained, not only predicting fatigue lives, but also in terms of fretting fatigue crack paths predictions.

2. Fretting fatigue experimental results

The contact pair used in the present paper corresponds to the usually called "cylindrical contact", in which a cylindrical contact pad of radius, R, is pressed against a flat surface. Fig. 1 shows a scheme for the device used to conduct the fretting fatigue tests. In that test setup, first the cylindrical contact pads are pressed against the flat surface of a dog-bone type fretting fatigue test specimen with a constant normal load N. The normal load is maintained almost perfectly constant thanks to the springs installed for this purpose (see Fig. 1**a**). Then, a fully reversed cyclic axial load of amplitude, P, is applied by means of a force controlled hydraulic actuator to the fretting fatigue test specimen. Due to the fretting fatigue device's flexibility, an in-phase tangential load, Q, is developed at the contact pads. The Q loads are measured directly by means of load cells developed in our laboratory for this specific purpose. An especial characteristic of the present device is, that for a certain value of P, the Q amplitude can be modified independently moving the

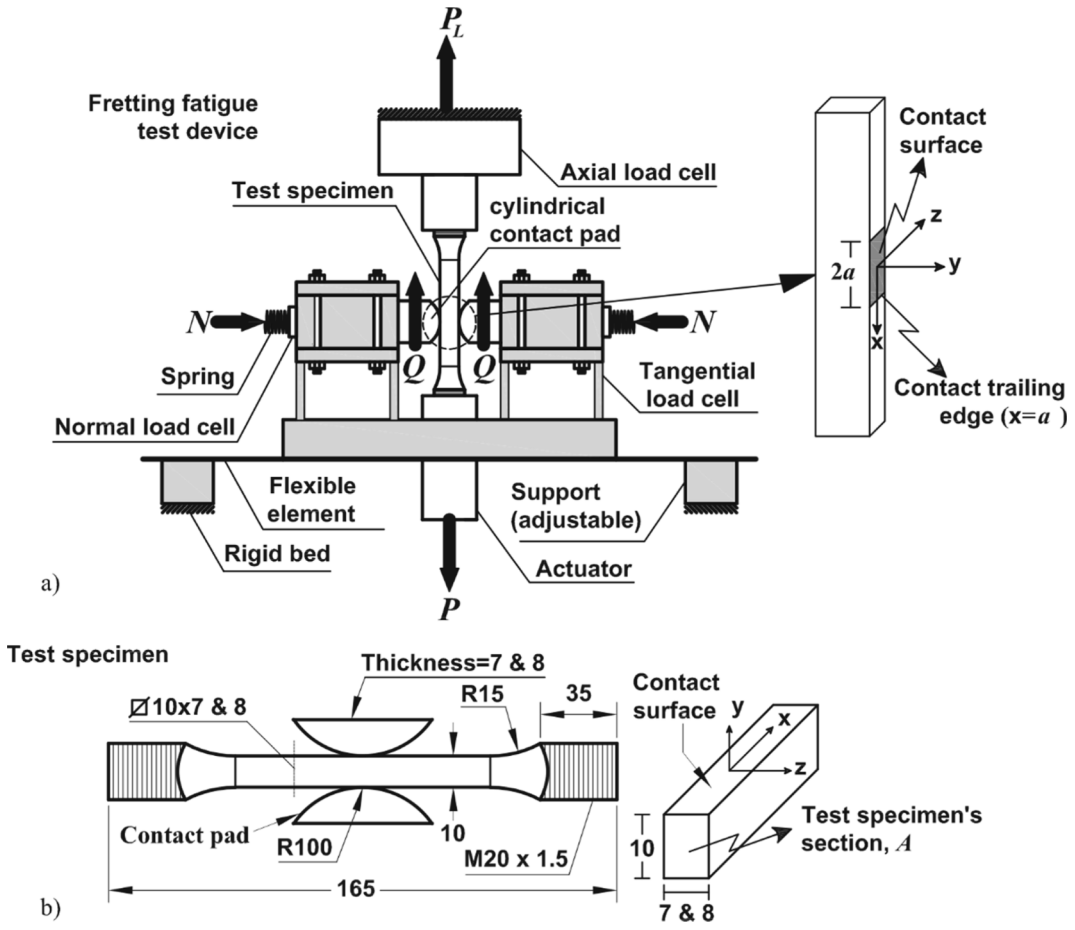

Fig. 1. a) Scheme of the fretting fatigue device used in the experimental campaign; b) main geometric characteristics –in mm- for the "dog bone" type fretting fatigue test specimens and contact pads.

adjustable supports (see Fig. 1**a**), and thus modifying device's compliance. The load P is obtained by means of the load cell on the top of the device, which measurement indicates the value $P_L = P + 2Q$, where Q *is* the tangential load measured at each side of the specimen. The uncertainty in the measurement of the normal, tangential and axial load cells for the loads applied are 1%, 2% and 0.5%, respectively.

Both contact pads and test specimens were made in aluminium alloy Al 7075-T651, which is widely used in the manufacture of aircraft components: wing skins, panels, covers, seat rear legs, and seat spreaders [33,34]. The chemical composition and main mechanical and fatigue properties for this material are shown in Table 1. Fig. 1**b** shows the specimen and contact pad dimensions. The results of two different experimental campaigns have been used, the only difference between both campaigns is the specimen thickness, 7 and 8 mm respectively. Experimental observations show that cracks initiate close to the contact trailing edge. Several crack initiation points are observed along the thickness of the specimen. These cracks merge at relatively small crack lengths and form a unique and uniform crack front [39].

Table 2 shows the fretting fatigue lives obtained in the experimental campaign with the corresponding fretting nominal loads. The actual loads have always been in the range of the nominal load ± 2%. In addition, the main theoretical parameters –using the plane strain Hertzian theory for elastic contacts- are also shown in the table in order to ease the comparison of the fretting conditions among different tests. In that table, a_H is the Hertzian theoretical contact semi-width and $\Delta\sigma_{xx}$ is the range of the direct/axial stress at the contact trailing edge, $x = a_H$ (see Fig. 1**a**). These two parameters are defined by the following equations [38]:

$$a_H = \sqrt{\frac{8N^*R(1-\nu^2)}{\pi E}} \tag{1}$$

$$\Delta\sigma_{xx} = \sigma + 4\mu p_0 \frac{c}{a_H}\sqrt{\left(\frac{a_H+e}{c}\right)^2 - 1} \tag{2}$$

Which in turn are obtained by means of $N^* = N/t$ (being t the test specimen thickness, 7 or 8 mm.), the amplitude of the test specimen bulk stress, $\sigma = P_a/A$, the maximum surface normal pressure, p_0, the contact stick zone half-width, c, the eccentricity of the stick zone, e, and the coefficient of friction μ; this last parameter is consider equal to 0.75 [39,40]. The expression for the above parameters are [38]:

$$p_0 = \frac{2N^*}{\pi a_H} \tag{3}$$

$$c = a_H\sqrt{1 - \left|\frac{Q}{\mu N}\right|} \tag{4}$$

$$e = \frac{R\sigma(1-\nu^2)}{\mu E} \tag{5}$$

3. Numerical models (FEM & XFEM).

The aforementioned test configuration is modelled in Abaqus software making use of the finite element method (FEM) and the extended version for crack modelling on a single mesh (XFEM). The reader is advised to read the following references for additional and concise details on the XFEM formulation [41–43]. Due to the nature of the fretting pair assembly and the relation between the thickness of the specimen and the contact width, it is possible to use, with a reasonable confidence, a 2D model assuming plane strain conditions [44]. Taking advantage of the symmetry of the test setup, only a contact pair is modelled. To reproduce the test performance, loads are applied in three steps (see Fig. 2**a**). The first step applies the normal load, N^*, and it is kept constant during the remaining steps. The second step applies the bulk stress, σ, to the right and the shear force, $Q^* = Q/t$, in the opposite direction. Finally, the third and last step applies the same values of σ and Q^*, but both in the opposite direction of step 2. Global dimensions and relevant parameters of the model are shown in Fig. 2**b**. Loads Q^* and N^* are applied to a master node that transfer the loads to all nodes lying on the top of the punch (see Fig. 3). The rotational movement of the master node is restricted. The bulk stress, is applied to the right side of the specimen. The horizontal movement of the left side of the specimen is restricted and symmetry conditions are applied to the remaining side.

The element used to mesh the geometry is quadrilateral with a bilinear formulation and plane strain features. The material is considered linear elastic. The contact pair is defined using the master–slave algorithm for contact between two surfaces. Lagrange multiplier formulation is considered in the contact pair to define the frictional behaviour of the parts assembled ($\mu = 0.75$). Contact of the crack faces in the XFEM model are considered as frictionless.

Considering the requirements of the fatigue model and the computational cost, two FEM models are defined (*Model A* and *Model B* in Fig. 3). *Model A* is used to obtain stress/strain fields near the trailing edge by means of FEM and is used for the crack initiation stage. *Model A* is also used at the propagation stage with XFEM for crack lengths below 150 μm, which will be called as early propagation stage. The mesh size of *Model A* is 1 μm × 1 μm around the trailing edge and it grows as it moves away from the refined zone or enriched area. In this manner, it is possible to capture the strong gradients that appear in this area and in the case of the crack propagation stage obtain more accurately the stress intensity factors (SIFs) of short cracks introduced by means of XFEM. On the other hand, *Model B* is only used with XFEM with the objective of obtaining the SIFs for cracks larger than 150 μm and propagate them up to failure. Therefore, the early propagated cracks obtained with *Model A*,

Table 1
Chemical composition (% weight) and main mechanical and fatigue properties for the Al 7075-T651.

(a) Chemical composition (% weight) [35]

%	Al	Zn	Mg	Cu	Fe	Si	Mn	Cr	Ti	Others
Max	91.4	6.1	2.9	2.0	0.5	0.4	0.3	0.28	0.2	0.05
Min	87.1	5.1	2.1	1.2	–	–	–	0.18	–	–

(b) Mechanical and fatigue properties

Young's modulus [35]	E	71 GPa	Ramberg-Osgood cyclic hardening coefficient [36]	K'	712 MPa
Poisson's ratio [35]	ν	0.33	Ramberg-Osgood cyclic hardening exponent [36]	n'	0.0410
Yield strength*	σ_y	503 MPa	fatigue strength coefficient [36]	σ'_f	995.4 MPa
Tensile strength*	σ_u	572 MPa	fatigue ductility coefficient [36]	ε'_f	0.0994
Mode I SIF threshold (R = 0.1) [13]	ΔK_{th}	2.2 MPa$\sqrt{m}$	fatigue strength exponent [36]	b	−0.0941
Pari's law coeff. (R = 0, m/cyc. and MPa$\sqrt{m}$) [37]	C	$8.831{\cdot}10^{-11}$	fatigue ductility exponent [36]	c	−0.578
Paris' law exp. (R = 0) [37]	m	3.322	Grain size*	d	50 μm

* Data obtained in our laboratory.

Table 2
Fretting fatigue lives, loads, thickness, and related Hertzian parameters for analysed tests.

Test	N (N)	Q (N)	σ (MPa)	N_f (Cycles)		t(mm)	a_H (mm)	c (mm)	p_0 (MPa)	e (mm)	$\Delta\sigma_{xx}$ (MPa)
1	4217	1543	110	88,216	89,376	8	1.30	0.93	258.6	0.18	800.2
2	5429	971	110	112,165	126,496	8	1.47	1.29	293.4	0.18	734.9
3	5429	1543	110	87,481	82,559	8	1.47	1.16	293.4	0.18	816.7
4	3006	971	150	60,040	59,234	8	1.10	0.83	218.3	0.25	785.5
5	3006	1543	150	19,223	39,408	8	1.10	0.62	218.3	0.25	866.0
6	3006	2113	150	34,904	41,002	8	1.10	0.27	218.3	0.25	938.1
7	4217	1543	150	50,369	39,001	8	1.30	0.93	258.6	0.25	890.9
8	5429	971	150	47,737	51,574	8	1.47	1.29	293.4	0.25	836.6
9	5429	1543	150	50,268	39,202	8	1.47	1.16	293.4	0.25	911.7
10	4750	1100	100	296,660	310,933	7	1.47	1.22	293.4	0.17	752.1
11	3690	1100	100	202,916	198,116	7	1.30	1.01	258.6	0.17	735.9
12	5800	850	70	577,540	676,704	7	1.63	1.46	324.2	0.12	640.9
13	5800	850	70	982,397	964,009	7	1.63	1.46	324.2	0.12	640.9
14	5800	1100	100	303,509	347,072	7	1.63	1.41	324.2	0.17	766.2
15	5800	850	80	333,660	397,855	7	1.63	1.46	324.2	0.13	669.0
16	5800	1350	110	167,324	165,421	7	1.63	1.35	324.2	0.18	830.9

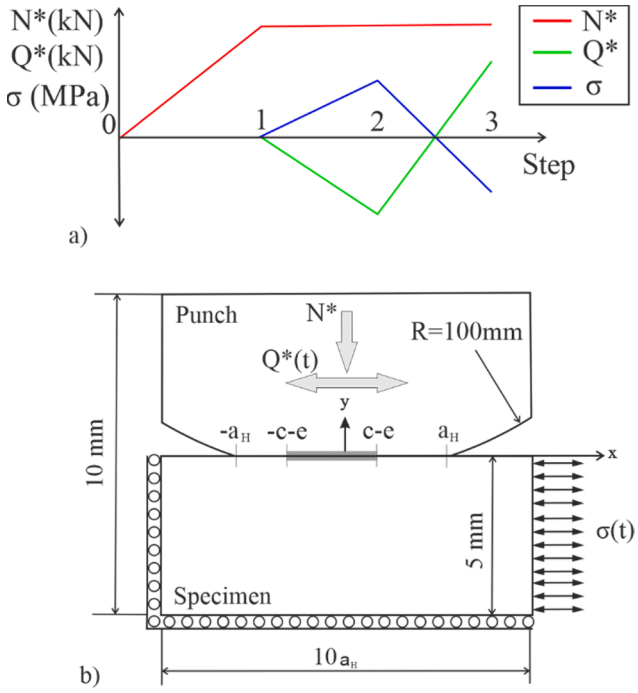

Fig. 2. a) Scheme of the load sequence; b) Main model parameters.

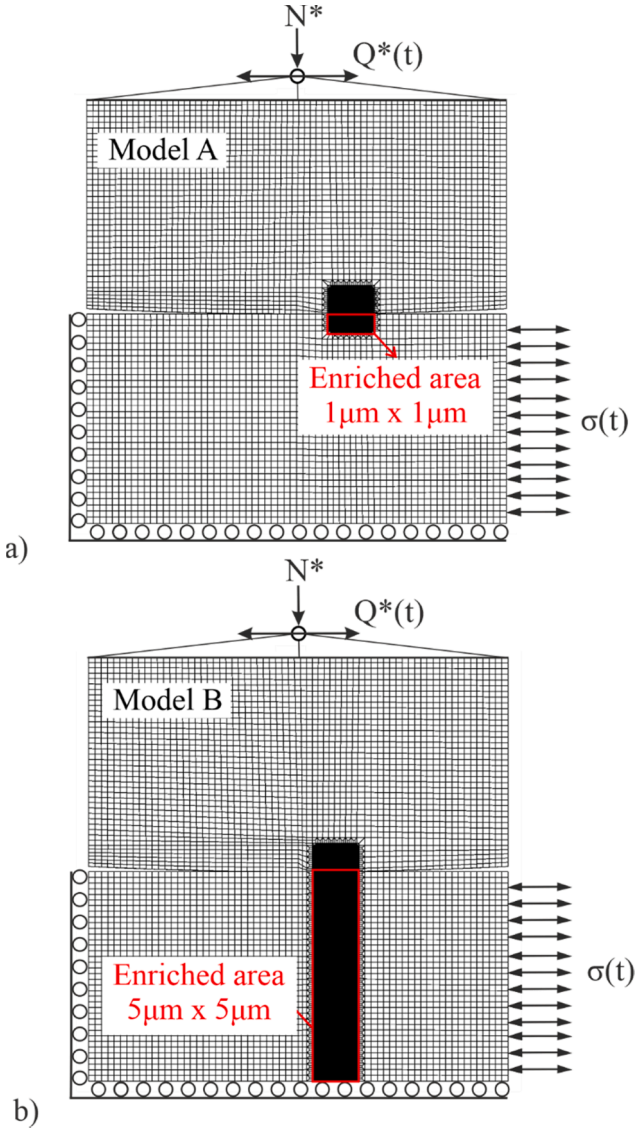

Fig. 3. Mesh and boundary conditions. a) Model A; b) Model B.

are later introduced in *Model B* to propagate them up to failure. Thus, a sufficiently large and wide area is necessary to propagate the crack up to the end of the specimen. As *Model B* is used only for large cracks, the element size in the refined area is 5 μm × 5 μm. This way it is possible to shorten significantly the computation time without losing accuracy. Although initial crack lengths studied in the current work are of the order of the material grain size, we assume a homogenous material. At such small scales it is important to take into account factors such as the microstructure and the dislocation density of the material; however, since the predictions at the initial crack stage will be made using the fatigue curve of the material, this phenomenon is inherently included in such curves.

4. Fatigue model

The proposed fatigue model is an improvement of one already developed by the authors [17–20], which could be considered as a variant of the critical distance method combined with LEFM, although its origin is based on the concept proposed by Socie et al [45]. The former model combines separately the initiation and propagation stages of cracks, without the necessity of predefine the crack length at which initiation ends, and propagation begins. In fact, the length defining the

limit between both phases is obtained during the process. In previous fretting related works the initiation phase analysed the number of cycles to generate a crack of a certain length, a_i, by means of the stress/strain field along a path perpendicular to the specimen surface and emanating from the contact trailing edge [29]. The number of cycles to generate this crack was obtained from a Coffin-Manson curve (ε-N). The result is a point of the curve (a_i-N_i) (see Fig. 4). Therefore, the curve is generated considering several discrete values of a_i. The curve (a_i-N_i) represents the number of cycles required to initiate/nucleate a crack of length a_i. Further details are developed in the next section. The proposed model improves the former in the sense that now the initial crack orientation is not predefined. That is, instead of considering the stress/strain fields along a path perpendicular to the surface with its origin at the trailing edge ($x = a_H$), it is obtained for different path orientations with its origin at different surface coordinates, selecting the most unfavourable. In this way it is possible to estimate the initial crack orientation angle and also the surface hot-spot without any previous assumption. In the case of fretting fatigue, it is well known that cracks initiate at a certain angle, pointing inside the contact zone, and not perpendicular to the surface [23,24].

In the propagation phase, the number of cycles to propagate the previous initial cracks a_i up to failure, are obtained by means of fracture mechanics based methods. Once a growth law is integrated from an initial crack a_i up to failure, the result is a point of the curve (a_i-N_p) (see Fig. 4). The curve is generated repeating the process for all the previously a_i defined. As it occurs with the initiation phase, former methods consider that the crack propagates completely straight. The proposed method avoids making this assumption and the crack propagation direction is estimated incrementally based on the stress/strains fields ahead the crack tip during a loading cycle based on the SWT parameter [26]. Therefore, the crack itself is able to follow the most critical path without any prior imposition.

Finally the sum of these two curves (a_i-N_i)+(a_i -N_p) give rise to the curve (a_i -N_T) (see Fig. 4). This curve should be understood as the total life estimated as a function of the crack length considered to delimitate the initiation and propagation phases, a_i. The minimum of the curve is considered as the fatigue life estimation, $N_T{}^* = N_i{}^* + N_p{}^*$, since it is the most unfavourable and conservative value of all possible combinations, and the length corresponding to this minimum is the proper crack initiation length, $a_i{}^*$.

4.1. Crack initiation phase

4.1.1. Multiaxial fatigue parameter estimation

This section defines the new procedure carried out to construct the curves (a_i-N_i) for each test. Recent works of the authors have demonstrated the capability of the SWT parameter to predict the initial crack orientation and also its subsequent propagation direction in fretting fatigue problems [25,26].

The procedure is described next. The traditional SWT parameter for uniaxial loading is shown in **Eq. (6)**. However due to the multiaxial characteristics of the loading states in fretting, **Eq. (7)** is considered to estimate the parameter, which is an extension of the original one for the case of non-proportional loading states and proposed by Marquis & Socie [46].

$$SWT = \sigma_{max}\frac{\Delta\varepsilon}{2} \tag{6}$$

$$SWT = \left(\sigma_n\frac{\Delta\varepsilon}{2}\right)_{max} \tag{7}$$

Where σ_n and $\Delta\varepsilon$ are the normal stress and the range of the normal strain to the material plane and along the loading cycle. The value of SWT is the product of these parameters at the plane orientation where it is maximum.

Fig. 5 shows a schematic representation of the method proposed based on the calculus of the SWT parameter with some modifications. At first, it is necessary to define a point at the surface where potentially a crack could nucleate which will be called critical point, the most common way is to consider that point at the contact trailing edge. This critical point is considered to be the origin of different material planes distributed homogeneously between $\theta_i = 90^\circ$ and $\theta_i = -90^\circ$ for a fixed radius a_i, defining the size of the influence area (see Fig. 5**a**). The radius of the influence area represents the initial crack length for which the SWT parameter will be obtained. The orientation, θ_i represents all possible directions of the nucleated crack, a_i. Now, the SWT parameter is calculated along each of these lines (defined by θ_i), but with the novelty that, the orientation of the material plane considered to evaluate the parameter is not the critical one, i.e., according to **Eq. (7)**, but the one that coincides with the orientation imposed by θ_i. For example, for the 0° plane (vertical) the stresses and strains used to obtain the SWT

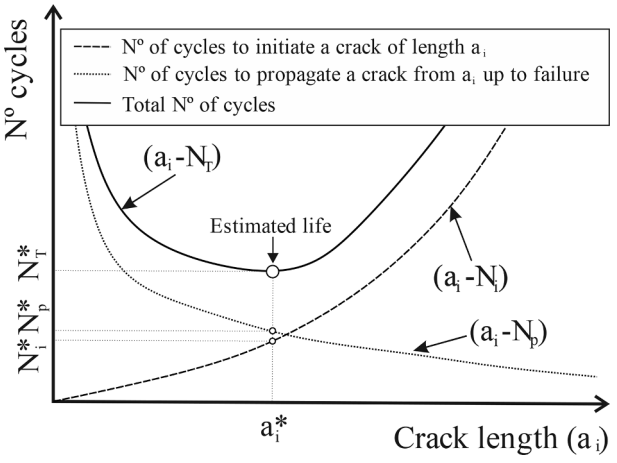

Fig. 4. Example of the curves obtained applying the fatigue model.

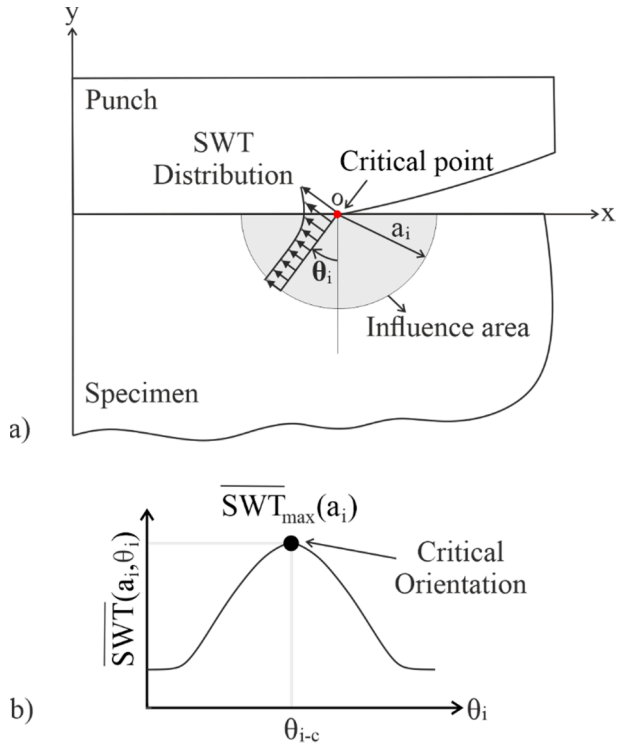

Fig. 5. Procedure to estimate the critical orientation angle, $\theta_{i-c}(a_i)$ and the maximum value of $\overline{SWT}(a_i, \theta_i)$.

parameter are σ_{xx} and ε_{xx} (perpendicular to the material line/plane), which potentially could produce a crack in vertical direction. With this procedure a SWT distribution (Fig. 5**a**) is obtained along each material line/plane. Next, the mean value of the SWT distribution along each line is calculated according to **Eq. (8)**.

$$\overline{SWT}(a_i,\theta_i)=\frac{1}{a_i}\int_o^{a_i} SWT(s,\theta_i)ds \tag{8}$$

Fig. 5**b** depicts the results of applying **Eq. (8)** for different θ_i. Finally the maximum value of the SWT parameter obtained from **Eq. (8)** is used to estimate the initiation life for the crack length a_i and the orientation where it is maximum is defined as $\theta_{i-c}(a_i)$. From now on references to *SWT* parameter are referred to maximum value obtained in **Eq. (8)**, see Fig. 5**b**.

The described procedure was also applied for different "critical points" surface positions and not only for $x/a_H = 1$. The analysed positions, x/a_H, ranged from 0.8 up to 1 with increments of 0.05. Noticing that the maximum value of $\overline{SWT}(a_i,\theta_i,x/a_H)$ is always obtained in the range x/a_H = [0.95–1]. Therefore, for the current model it is not necessary to define the critical point at the contact surface as it is possible to obtain its x/a_H coordinate as part of the procedure. However, due to the results obtained and to avoid more variables the critical point could be considered at the contact trailing edge as a rule of thumb.

4.1.2. *Construction of initiation curves.*

The number of cycles to nucleate a crack of length, a_i, will be obtained by means of the fatigue curve of the material in plain fatigue with no stress gradient. To achieve this goal, the ε-N_T curve of the material is expressed in terms of the SWT parameter (**Eq. (9)**).

$$SWT=\frac{\dot{\sigma_f}^2}{E}(2N_T)^{2b}+\dot{\sigma_f}\dot{\varepsilon_f}(2N_T)^{b+c} \tag{9}$$

It is important to note that this curve represents the cycles up to what in tests was defined as failure, which means that initiation and propagation cycles are joined in the term N_T. In the current work the failure of the tests considered for the Coffin-Manson curve defines the number of cycles when separation of the specimen in two parts is occurred [36], according to [49]. Nevertheless, for the objective of the current phase it is necessary to construct a series of curves to obtain the number of cycles (N_i) required to nucleate a specific crack length (a_i) for each SWT level.

To do so **Eq. (10)** is applied for all possible SWT values and the initiation length, a_i. Which means that for each a_i a new curve is generated. From now on these curves will be called *SWT-*N_i. Fig. 6 depicts an example of an initiation curve obtained according to **Eq. (10)**.

$$N_i(SWT,a_i)=N_T(SWT)-N_p(SWT,a_i) \tag{10}$$

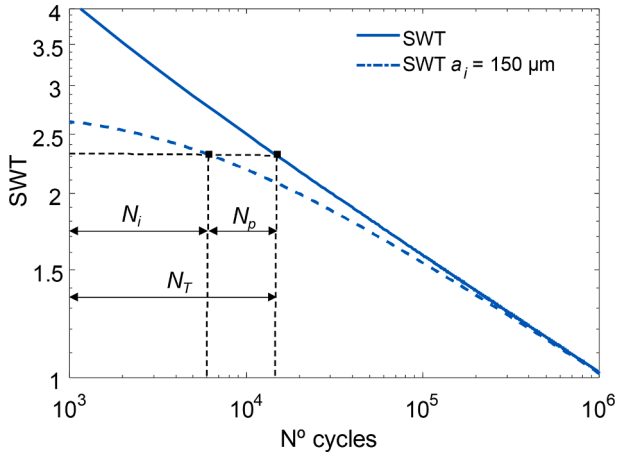

Fig. 6. a) Creation of initiation curves *SWT-*N_i with propagation computed via the Paris law.

In **Eq. (10)** N_i is the number of cycles to initiate/nucleate the crack a_i, N_T is the total number of cycles obtained from **Eq. (9)**, N_p is the number of cycles to propagate the crack a_i up to failure (a_f) integrating a crack growth law. For comparison purposes, the propagation cycles are computed using the Pariscrack growth law (**Eq. (11)**) and also the Vallellanós modification that includes the effect of microcracks (**Eq. (12)**) [48].

$$\frac{da}{dN_p}=C(\Delta K)^m \tag{11}$$

$$\frac{da}{dN_p}=C(\Delta K)^m-C\left(\Delta K_{th}\left(\frac{a^f}{a^f+a_0^f-l_0^f}\right)^{\frac{1}{2f}}\right)^m \tag{12}$$

Where the parameter l_0 is the distance from the surface to the first microstructural barrier, defined as half of the grain size d, and the exponent f is equal to 2.5 [48].

The fatigue curve of the material used in the current work is the one defined by **Eq. (9)** and the material parameters of Table 1**.** According to the authors, the fatigue curve was obtained with cylindrical specimens with a diameter of 7 mm and stress ratio R = -1 via uniaxial tests and the failure was considered when the specimens completely broke [36]. With this information and also the cyclic Ramber – Osgood equation (**Eq. (13)**) it is possible to translate the values of SWT (according to **Eq. (6)**) to $\Delta\sigma$. Knowing the value of $\Delta\sigma$ and bearing in mind that the growth law constants were obtained for R = 0 it is possible to compute $\Delta K_I(a)=\frac{\Delta\sigma}{2}Y\sqrt{\pi a}$ taking into account that $\frac{\Delta\sigma}{2}=\sigma_{max}$. Where the corrective factor, Y, is obtained from Nasgro software, considering a semi-elliptical crack growing in a cylindrical specimen and a ranges from a_i up to a_f.

$$\frac{\Delta\varepsilon}{2}=\frac{\Delta\sigma}{2E}+\left(\frac{\Delta\sigma}{2K'}\right)^{\frac{1}{n'}} \tag{13}$$

Integrating the ΔK_I values according to **Eq. (11)** or **Eq. (12)** and applying **Eq. (10)** it is possible to generate the so called initiation curves for which an example is depicted in Fig. 6**.** It is important to note that, there is a stress level depending on the initial crack length considered, from which the propagation cycles, N_p, are higher than the estimated total cycles, N_T, obtained from **Eq. (9)**. In these cases, the initiation cycles computed according to **Eq. (10)** are negative, which is a nonsense. Therefore, a value of one cycle is assigned to the initiation phase in these stress levels.

Then with the SWT value obtained in Section 4.1.1 it is possible to obtain the number of cycles, N_i, required to initiate a crack of length a_i, from the (*SWT-*N_i) curve associated to the initial crack length a_i, previously generated. Therefore, the pair of data a_i and N_i obtained, define a point of the curve (a_i- N_i) of Fig. 4**.**

Finally, to generate the whole curve a_i-N_i *(see* Fig. 4*)*, Sections 4.1.1 and 4.1.2 should be repeated for all the desired a_i lengths. Besides, the value of $\theta_{i-c}(a_i)$ is also obtained for each a_i.

4.2. *Crack propagation phase. Curves* a_i-N_p

The crack propagation phase is studied via XFEM by means of Abaqus software. This numerical technique allows the simulation of cracks, which are introduced after the meshing process. Due to this feature, it is not necessary to develop different models with different crack sizes and fine meshes at the crack tip [41]. To estimate the crack propagation lifetime, SIFs in mode I and II are computed via the interaction integral method implemented in Abaqus for each loading step. In the case of Abaqus software it is possible to define the crack tip and several contours to evaluate the integral and automatically obtain the SIFs. Once the SIFs are known it is possible to estimate the crack propagation lifetime integrating any crack growth law. In order to take into account both SIFs modes, an equivalent ΔK_{eq} (**Eq. (14)**) is obtained using the expression proposed by Tanaka et al. [47].

$$\Delta K_{eq} = \sqrt[4]{\Delta K_I^4 + 8\Delta K_{II}^4} \quad (14)$$

The crack propagation orientation method applied in the current work is based on the procedure developed at the crack initiation stage [25]- [26]. A schematic view of the proposed methodology is depicted in Fig. 7. The first step is to introduce an initial crack length and orientation in the numerical model, a_i at its corresponding θ_{i-c}. Once the XFEM models is numerically solved and the stress/strain fields are known, the SWT procedure described earlier in Section 4.1.1 is now applied at the postprocessor stage moving the critical point at the contact surface (see Fig. 5**a**) to the crack tip, O_1 in Fig. 7**a**. At this stage, instead of evaluating the SWT parameter along the material planes defined by θ, the parameter is evaluated at different points ahead of the crack tip at a constant distance r^* (black dots in Fig. 7**a**). With this modification the effect of the singularity at the crack tip is avoided. We assume that the crack will not go backwards. The orientation with the highest value of the SWT parameter is considered the more prone to propagate the crack (θ_{p-c} in Fig. 7**b**). With the new orientation and defining the crack propagation increment, Δa, the next crack path increment and tip are determined, being the next critical point of the method at O_2. The procedure should be repeated up to the desired crack length or up to final crack length which results in fracture of specimen. In the current work, the final fracture is considered when the crack has crossed the entire specimen. It is important to note that the value of the parameter r^* does not play an important role at the propagation stage. Due to the fact that the stress and strain fields ahead of the crack tip are proportional to $1/\sqrt{r^*}$ as demonstrated in Ref. [25]. However, in the current work a value of 100 μm is considered.

For each crack increment, Δa, from a_i up to a_f the SIFs are obtained and an equivalent value is calculated according to **Eq. (14)**, thus knowing the evolution of the SIFs during the crack propagation stage $\Delta K_{eq}(a)$, in function of the total crack length $a = a_i + s$, where s is a coordinate that runs along the propagated crack with its origin at O_1 (see Fig. 7**a**). During the incremental process the estimated crack profile is drawn automatically. Finally applying the crack growth laws of **Eq. (11)** and **Eq. (12)**, the number of cycles, N_p, required to propagate an initial crack a_i up to failure are obtained. Therefore, the pair of data a_i and N_p obtained, define a point of the curve (a_i- N_p) of Fig. 4. The described procedure should be repeated for all the initial crack lengths a_i defined in the initiation section. Thus drawing the curve (a_i- N_p) of Fig. 4.

The minimum value of the sum of both (a_i- N_i) and (a_i- N_p) curves is the estimated life (N_T*) for the specific test and its corresponding length, a_i*, is the crack length that defines the point of change from initiation phase to propagation phase.

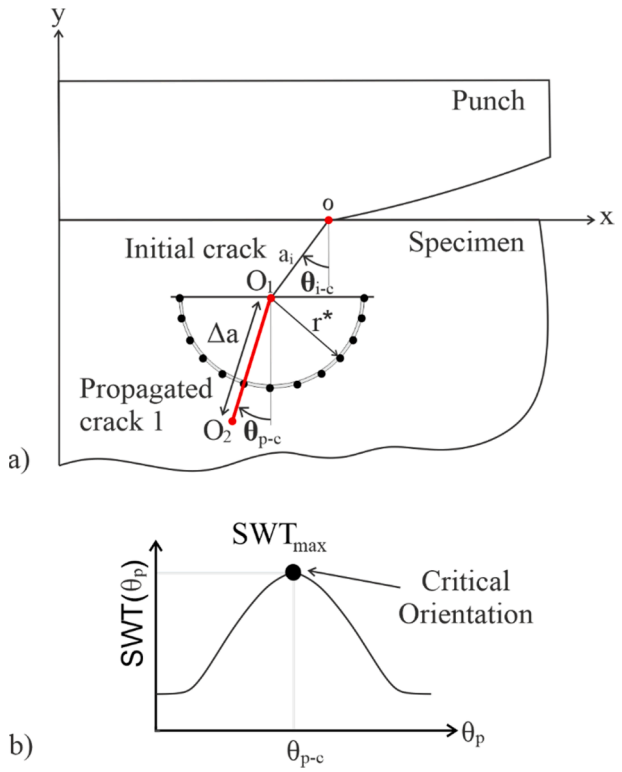

Fig. 7. Procedure to estimate the critical orientation angle, θ_{p-c}.

5. Results

In this section we show and comment on the results obtained in terms of life estimation and crack path predictions for the tests shown in Table 2. First of all, some of the predicted crack paths obtained while creating the curves (a_i-N_i) and (a_i-N_p) are compared with real crack profiles. Later the results obtained for the life estimation are shown and commented.

5.1. Crack path predictions

In the case of the crack initiation phase, for which FEM is used in *Model A* (see Fig. 3**a**), crack initiation lengths, a_i, ranging from 10 μm to 150 μm are analysed. The corresponding value of $\theta_{i-c}(a_i)$ is obtained for each length, noticing that independently of the crack initiation length, the values are almost the same. That is, the variation of the parameter θ_{i-c} obtained is minimum independently of the test, less than 3°.

In the case of the early crack propagation phase, for which XFEM is used in *Model A* (see Fig. 3**a**), each of the initial cracks defined previously are propagated following the proposed method, assuming crack increments of $\Delta a_p = 10\mu m$ up to a total crack depth $a = 150\mu m$. Noticing that these early crack propagation profiles predicts approximately the same crack paths as those obtained with the initiation stage for the same total crack length, although the results depends on each specific test configuration.

Finally large crack propagation, from $a = 150\mu m$ up to the limit of the specimen, imposing now $\Delta a_p = 150\mu m$, are obtained with XFEM from *Model B* (see Fig. 3**b**) in which early propagated cracks are introduced to continue with its propagation up to failure.

An example of some crack profiles obtained for *Test 12* and *Test 16* are shown in Fig. 8 in which also real crack profile measurements are included [25], two measurements for Test 12 and one for Test 16. The

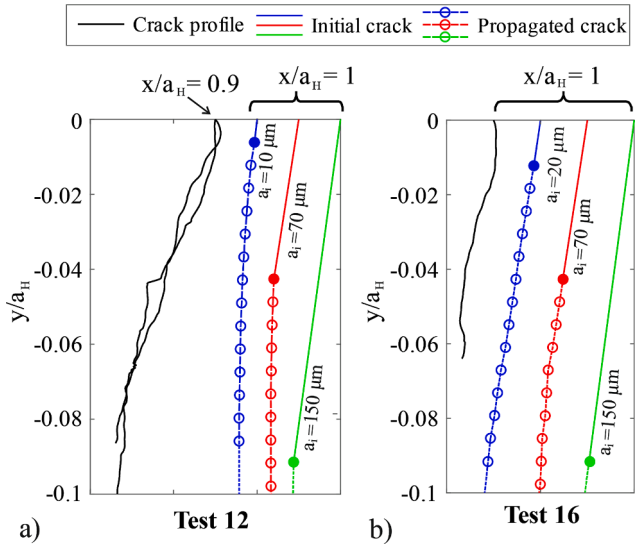

Fig. 8. Example of three crack paths estimated by the proposed method a) Test 12, b) Test 16.

predicted cracks profiles of Fig. 8 are shown separately for a better visualization. Three cracks are shown with different combination of crack initiation and propagation lengths for each test. Each crack profile defines a single point of the curve (a_i -N_T) of Fig. 4**.** The scale of the abscissa axis is the same as the ordinate axis in order to see the crack in true magnitude. Continuous lines represent the initiation phase and discontinuous lines represent the propagation phase. Circles represent the crack increments (in this figure only early crack propagation is observed). Filled circles indicates the length, a_i, where crack initiation finishes and propagation begins. It can be observed that the cracks orientations are in reasonable agreement with actual crack profiles. In the case of Test 12 the experimental slope for the cracks in the range showed in Fig. 8**a** is approximately 16° which is significant larger than the value of 3° obtained for the blue crack (which is the one with the most unfavourable value for total life). In the case of Test 16 the difference between estimated and experimental cracks is negligible, less than 2°, being the slope of the predicted crack 6°. It is important to take into account that both in the model and in the real crack it becomes almost vertical from a certain distance, but this distance is different in each one and that makes it difficult to compare in a quantitative way. This different behaviour, depending on the test, is due to the surface contact point of initiation of actual cracks, in *Test 16* both predicted and actual crack emanate approximately from the contact trailing edge, $x = a_H$. However, in the case of *Test 12*, the predicted cracks emanate approximately from the trailing edge and the actual one was found slightly inside the sliding zone, specifically at $x/a_H = 0.9$ and this is the reason why it has a higher slope. The crack propagation criterion is able to capture this effect and predict a better crack orientation estimation applying Section 4.1.1 at $x/a_H = 0.9$, with a value of 25°. However, numerical results always indicate that the most unfavourable point of the contact surface is at or close to the trailing edge. Therefore, this observation seems to indicate that there is some effect during the test that is not being taken into account since, according to experimental results, cracks not always emanate close to the trailing edge. In any case, the predicted cracks obtained are in good agreement with those observed and provides a physical meaning to the proposed model.

5.2. Life predictions

The results in terms of fatigue life predictions estimated for tests in Table 2 are shown in this section. First of all, an example of the curves obtained according to Fig. 4 are shown in Fig. 9 for some tests of Table 2 and considering the Pariś crack growth law for the propagation phase.

Next, Table 3 shows the numeric results obtained after applying the proposed method. The initiation, propagation and therefore total cycles, depends on the crack growth law considered. As mentioned earlier, in the current work two different laws have been considered with comparison purposes (see **Eq. (11)** and **Eq. (12)**). The results obtained with both laws are shown in Table 3. It is important to note that the initiation phase depends also on the crack growth law used to compute the *SWT-N_i* curves. To be consistent if the Paris crack growth law is used to compute the *SWT-N_i* curves, the same law is used to estimate the test crack propagation cycles. Likewise, with the Vallellano law.

If the value of a_i* is analysed it ranges between 10 μm and 50 μm without any clear pattern. However, all the values obtained are of the order of the grain size of the material. In the case, of the crack initial orientation, in a general way it could be said that it is independent of the loading state, obtaining values ranging from 5° to 9°. In the specific cases in which the minimum of the total curve is obtained at 10 μm, an additional point of the curve was studied for an initial crack length of 5 μm, without any change in the results. Therefore, it is reasonable to consider 10 μm as the minimum crack size to be studied in the proposed model.

Finally, the estimated total fatigue lives of Table 3 are depicted in Fig. 10 vs. the experimental ones from Table 2. The results on the left of Table 3 are obtained considering the Pariś law and the results on the right are those obtained with the Vallellano crack growth law. Independently of the propagation method used, the estimated lives are in good agreement with the experimental ones. However, it seems to be that the use of the Pariś law yields slightly better results than the Vallellanós one. Even there are two points (Test 13) in Fig. 10**b** that are indicated as a run-out, actually what happens to this estimation is that due to the form of **Eq. (12)**, the value of da/dN_p is negative because $\Delta K_{eq} < \Delta K_{th}$ and therefore the method predict a non-propagating crack. In order to quantify which method predicts best results, the data is adjusted with a regression line to a curve of the type $N_f = N^*_T$ (Discontinuous line in Fig. 10). In the case in which the Vallelanós crack growth is used, the fitting does not take into account the results of Test 13. In terms of the squared correlation factor, R^2, the results obtained with the Pariślaw are better than those of Vallellanós law as can be seen in Fig. 10.

6. Conclusions

The current work presents a fretting fatigue model based on the SWT critical plane parameter. Due to the formulation of the model, decisions on crack orientation as well as the length of the crack at which the initiation phase ends and the propagation phase begins are estimated by the model. For this purpose, it has been analysed which combination of initiation and propagation is the most unfavourable in terms of total life, taking into account also the self-steered crack path, which is obtained during the calculation process. The crack paths obtained draw a crack profile in agreement with those observed experimentally, thus providing also a physical meaning to the model. To estimate the total fatigue life,

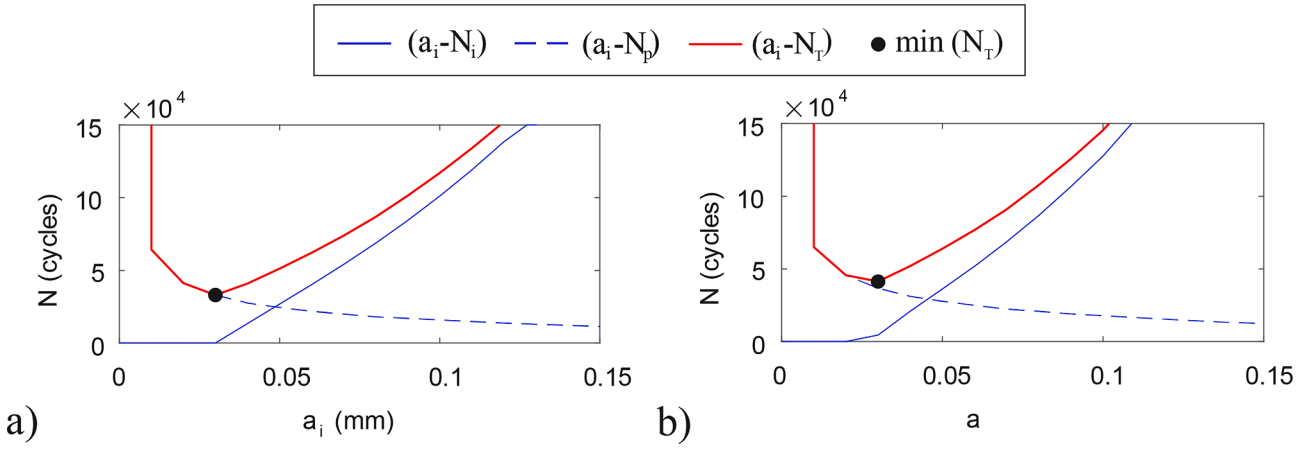

Fig. 9. Initiation, propagation and total life curves with Pariś law. a) Test 5, b) Test 7.

Table 3
Estimated crack initiation length and orientation, initiation, propagation and total life for different crack growth laws.

		Paris' Crack Growth Law				Vallellano's Crack Growth Law					
Test	θ_i* (°)	a_i*(μm)	N_i*	N_p*	N_T*	a_i*(μm)	N_i*	N_p*	N_T*	N_f (Cycles)	
1	6	20	1	40,102	40,103	30	278	37,412	37,690	88,216	89,376
2	9	10	9470	205,907	215,377	20	35,020	425,780	460,800	112,165	126,496
3	6	20	1	75,313	75,314	20	1	88,569	88,570	87,481	82,559
4	6	20	1	86,474	86,475	40	11,400	110,700	122,100	60,040	59,234
5	6	40	882	27,519	28,401	40	1	30,219	30,220	19,223	39,408
6	6	40	3267	20,868	24,135	40	1	22,325	22,326	34,904	41,002
7	7	40	4743	31,088	35,831	40	215	34,915	35,130	50,369	39,001
8	6	30	9864	113,470	123,334	50	48,430	149,770	198,200	47,737	51,574
9	6	40	1367	56,705	58,072	40	1411	62,819	64,230	50,268	39,202
10	6	10	1	116,914	116,915	10	1	134,899	134,900	296,660	310,933
11	6	20	1	66,344	66,345	20	1	68,909	68,910	202,916	198,116
12	6	10	311,400	444,515	755,915	50	1	808,499	808,500	577,540	676,704
13	8	10	753,300	493,918	1,247,218	–	–	–	>1E + 7	982,397	964,009
14	6	10	1	153,348	153,349	20	5119	160,581	165,700	303,509	347,072
15	6	10	198,800	316,106	514,906	40	1	478,799	478,800	333,660	397,855
16	6	20	11,910	76,678	88,588	20	1	62,369	62,370	167,324	165,421

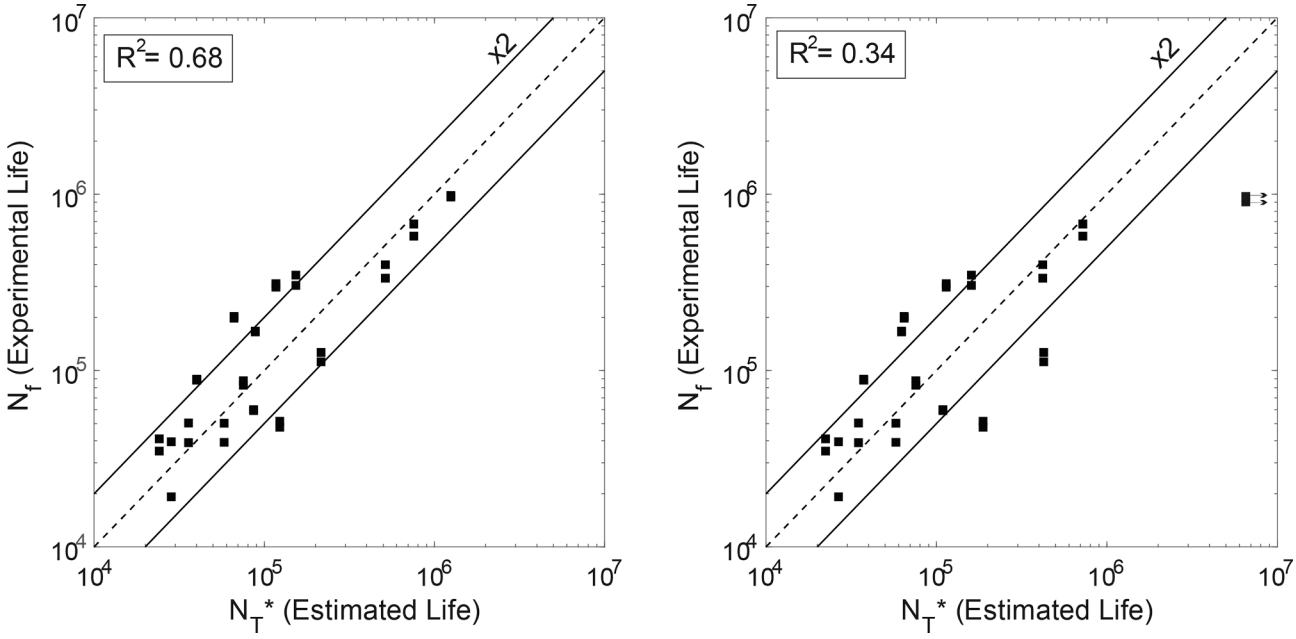

Fig. 10. Estimated fatigue lives vs. experimental fatigue lives. a) Paris' crack growth law, b) Vallellanós crack growth law.

two different propagation laws have been used. Observing that by using the Pariś law, which is a very simple approach, slightly better results are obtained if compared with those obtained with the Vallellanós law. Although the differences between the predicted lives are not that high.

Declaration of Competing Interest

The authors declare that they have no known competing financial interests or personal relationships that could have appeared to influence the work reported in this paper.

References

[1] Waterhouse R. Fretting fatigue. U.K: Applied science publishers; 1981.
[2] Jimenez-Peña C, Talemi RH, Rossi B, Debruyne D. Investigations on the fretting fatigue failure mechanism of bolted joints in high strength steel subjected to different levels of pre-tension. Tribol Int 2017;108:128–40. https://doi.org/10.1016/j.triboint.2016.11.014.
[3] C.R.F. Azevedo, A.M.D. Henriques, A.R. Pulino Filho, J.L.A. Ferreira, J.A. Araújo, Fretting fatigue in overhead conductors: rig design and failure analysis of a Grosbeak aluminium cable steel reinforced conductor, Eng. Fail. Anal. 16 (1) (2009) 136–151.
[4] Y.B. Zhang, L.T. Lu, L. Zou, D.F. Zeng, J.W. Zhang, Finite element simulation of the influence of fretting wear on fretting crack initiation in press-fitted shaft under rotating bending, Wear 400 (2018) 117–183, https://doi.org/10.1016/j.wear.2018.01.008.
[5] GOLDEN, Patrick J. Development of a dovetail fretting fatigue fixture for turbine engine materials. International Journal of Fatigue, 2009, vol. 31, no 4, p. 620-628.
[6] M. Ciavarella, G. Demelio, A review of analytical aspects of fretting fatigue, with extension to damage parameters, and application to dovetail joints, Int. J. Solids Struct. 38 (10-13) (2001) 1791–1811.
[7] Araújo JA, Nowell D, Vivacqua RC. The use of multiaxial fatigue models to predict fretting fatigue life of components subjected to different contact stress fields. Fatigue Fract. Eng. Mater. Struct. 2004;27:967–78.
[8] C. Vallellano, J. Domínguez, A. Navarro, Predicting the fretting fatigue limit for spherical contact, Eng. Fail. Anal. 11 (5) (2004) 727–736.
[9] J. Araujo, L. Susmel, D. Taylor, J. Ferro, E. Mamiya, On the use of the Theory of Critical Distances and the Modified Wöhler Curve Method to estimate fretting fatigue strength of cylindrical contacts, Int. J. Fatigue 29 (1) (2007) 95–107.
[10] Jesús Vázquez, Andrea Carpinteri, Luis Bohórquez, Sabrina Vantadori, Fretting fatigue investigation on Al 7075–T651 alloy: Experimental, analytical and numerical analysis, Tribol. Int. 135 (2019) 478–487.
[11] Sabrina Vantadori, Jesús Vázquez Valeo, Andrea Zanichelli, Fretting fatigue and shot peening: a multiaxial fatigue criterion including residual stress relaxation, Tribol. Int. 151 (2020) 106537, https://doi.org/10.1016/j.triboint.2020.106537.
[12] Yoshiharu Mutoh, Jin-Quan Xu, Fracture mechanics approach to fretting fatigue and problems to be solved, Tribol. Int. 36 (2) (2003) 99–107, https://doi.org/10.1016/S0301-679X(02)00136-6.

[13] Sergio Muñoz, Carlos Navarro, Jaime Domínguez, Application of fracture mechanics to estimate fretting fatigue endurance curves, Eng. Fract. Mech. 74 (14) (2007) 2168–2186.
[14] Da-Sheng Wei, Yan-Rong Wang, Analysis of fretting fatigue life of dovetail assemblies based on fracture mechanics method, Eng. Fail. Anal. 25 (2012) 144–155.
[15] Eduardo Martins Fontes do Rêgo, Marcelo Avelar Antunes, Antonio Carlos de Oliveira Miranda, A methodology for fretting fatigue life estimation using strain-based fracture mechanics, Eng. Fract. Mech. 194 (2018) 24–41.
[16] Matthew P. Szolwinski, Thomas N. Farris, Mechanics of fretting fatigue crack formation, Wear 198 (1-2) (1996) 93–107.
[17] C. Vallellano, J. Vázquez, A. Navarro, J. Domínguez, A micromechanical model for small fatigue crack growth: an approach based on two threshold conditions. Fatigue Fract. Eng. Mater. Struct. 2009;32:515–24.
[18] J. Vázquez, C. Navarro, J. Domínguez, On the estimation of fatigue life in notches differentiating the phases of crack initiation and propagation, Fatigue Fract. Eng. Mater. Struct. 33 (2010) 22–36.
[19] C. Navarro, J. Vázquez, J. Domínguez, A general model to estimate life in notches and fretting fatigue, Eng. Fract. Mech. 78 (8) (2011) 1590–1601.
[20] J. Vázquez, C. Navarro, J. Domínguez, A model to predict fretting fatigue life including residual stresses, Theor. Appl. Fract. Mech. 73 (2014) 144–151.
[21] Reza Hojjati-Talemi, Magd Abdel Wahab, Eugenio Giner, Mohamad Sabsabi, Numerical Estimation of Fretting Fatigue Lifetime Using Damage and Fracture Mechanics, Tribol. Lett. 52 (1) (2013) 11–25.
[22] M.H. El Haddad, K.N. Smith, T.H. Topper, Fatigue Crack Propagation of Short Cracks, J. Eng. Mater. Technol. 101 (1979) 42–46.
[23] J. Vázquez, C. Navarro, J. Domínguez, Analysis of fretting fatigue initial crack path in Al7075-T651 using cylindrical contact, Tribol. Int. 108 (2017) 87–94.
[24] C. Navarro, J. Vázquez, J. Domínguez, Nucleation and early crack path in fretting fatigue, Int. J. Fatigue 100 (2017) 602–610.
[25] L. Bohórquez, J. Vázquez, C. Navarro, J. Domínguez, On the prediction of the crack initiation path in fretting fatigue, Theor. Appl. Fract. Mech. 99 (2019) 140–146.
[26] Diego Erena, Jesús Vázquez, Carlos Navarro, Reza Talemi, Numerical study on the influence of artificial internal stress relief groove on fretting fatigue in a shrink-fitted assembly, Tribol. Int. 151 (2020) 106443, https://doi.org/10.1016/j.triboint.2020.106443.
[27] Ali Fatemi, Darrell F. Socie, A critical plane approach to multiaxial fatigue damage including out-of-phase loading, Fatigue Fract. Eng. Mater. Struct. 11 (3) (1988) 149–165.
[28] R.N. Smith, P. Watson, A. Topper, Stress-strain function for the fatigue of metals, J. Mater. JMSLA 5 (1970) 767–778.
[29] C. Navarro, S. Munoz, J. Dominguez, On the use of multiaxial fatigue criteria for fretting fatigue life assessment, Int. J. Fatigue 30 (1) (2008) 32–44, https://doi.org/10.1016/j.ijfatigue.2007.02.018.
[30] S. Munoz, H. Proudhon, J. Dominguez, S. Fouvry, Prediction of the crack extension under fretting wear loading conditions, Int. J. Fatigue 28 (12) (2006) 1769–1779.
[31] S. Fouvry, D. Nowell, K. Kubiak, D.A. Hills, Prediction of fretting crack propagation based on a short crack methodology, Eng. Fract. Mech. 75 (6) (2008) 1605–1622.
[32] A. de Pannemaecker, S. Fouvry, J.Y. Buffiere, M. Brochu, Modelling the fretting fatigue crack growth: From short crack correction strategies to microstructural approaches, Int. J. Fatigue 117 (2018) 75–89.
[33] Ali Merati, Graeme Eastaugh, Determination of fatigue related discontinuity state of 7000 series of aerospace aluminum alloys, Eng. Fail. Anal. 14 (4) (2007) 673–685.
[34] Frank Czerwinski, Controlling the ignition and flammability of magnesium for aerospace applications, Corros. Sci. 86 (2014) 1–16.
[35] Alloy 7075 Plate and Sheet: Alcoa Mill Products: SPD-10-037, 2001.
[36] NIMS Fatigue Data Sheet No. 123: Data sheet on low-and high-cycle fatigue properties of A7075-T6 (Al-5.6Zn-2.5Mg-1.6Cu) Aluminium alloy. National Institute for Materials Sciences, Japan, 2017. ISSN 1347-3093.
[37] Military Handbook - MIL-HDBK-5H: Metallic Materials and Elements for Aerospace Vehicle Structures, U.S. Department of Defense, ISBN 978-1-59124-543-8.
[38] J. Vázquez, C. Navarro, J. Domínguez, A new method for obtaining the stress field in plane contacts, Int. J. Solids Struct. 49 (26) (2012) 3659–3665.
[39] Vicente Martín, Jesús Vázquez, Carlos Navarro, Jaime Domínguez, Fretting-Fatigue Analysis of Shot-Peened Al 7075–T651 Test Specimens, Metals (Basel) 9 (5) (2019) 586, https://doi.org/10.3390/met9050586.
[40] Vicente Martín, Jesús Vázquez, Carlos Navarro, Jaime Domínguez, Effect of shot peening residual stresses and surface roughness on fretting fatigue strength of Al 7075–T651, Tribol. Int. 142 (2020) 106004, https://doi.org/10.1016/j.triboint.2019.106004.
[41] T. Belytschko, T. Black, Elastic crack growth in finite elements with minimal remeshing, Int. J. Numer. Meth. Engng. 45 (1999) 601–620, https://doi.org/10.1002/(SICI)1097-0207(19990620)45:5<601::AID-NME598>3.0.CO;2-S.
[42] R. Hojjati-Talemi, M. Abdel Wahab, J. De Pauw, P. De Baets, Prediction of fretting fatigue crack initiation and propagation lifetime for cylindrical contact configuration, Tribol. Int. 76 (2014) 73–91, https://doi.org/10.1016/j.triboint.2014.02.017.
[43] E. Giner, M. Sabsabi, J.J. Ródenas, Fuenmayor F. Javier, Direction of crack propagation in a complete contact fretting-fatigue problem, Int J Fatig 58 (2014) 172–180, https://doi.org/10.1016/j.ijfatigue.2013.03.001.
[44] Jesús Vázquez, Carlos Navarro, Jaime Domínguez, Two dimensional versus three dimensional modelling in fretting fatigue life prediction, J. Strain Anal. Eng. Des. 51 (2) (2016) 109–117.
[45] Darrell F. Socie, Jodean Morrow, Wen-Ching Chen, A procedure for estimating the total fatigue life of notched and cracked members, Eng. Fract. Mech. 11 (4) (1979) 851–859.
[46] MARQUIS, G. B.; SOCIE, D. F. Multiaxial fatigue. 2003.
[47] Keisuke Tanaka, Fatigue crack propagation from a crack inclined to the cyclic tensile axis, Eng. Fract. Mech. 6 (3) (1974) 493–507.
[48] C. Vallellano, J. Dominguez, A. Navarro, On the estimation of fatigue failure under fretting conditions using notch methodologies, Fatigue Fract. Eng. Mater. Struct. 26 (5) (2003) 469–478, https://doi.org/10.1046/j.1460-2695.2003.00649.x.
[49] ASTM E606 / E606M-21, Standard Test Method for Strain-Controlled Fatigue Testing, ASTM International, West Conshohocken, PA, 2021, www.astm.org..